Electrostatic Assembly of Gold Colloidal Nanoparticles on Organosilane Monolayers Patterned by Microcontact Electrochemical Conversion

Chi-Fan Chen, Shien-Der Tzeng, Meng-Hsien Lin, and Shangjr Gwo*

Department of Physics and Institute of MEMS, National Tsing-Hua University, Hsinchu 300, Taiwan, R.O.C.

Received March 9, 2006. In Final Form: June 26, 2006

A new approach is introduced for electrostatically guided adsorption of colloidal nanoparticles onto a patterned self-assembled monolayer (SAM) with feature sizes ranging from nm to mm. Patterning of the adsorption templates is realized by electric-field-induced anodic oxidation of aminosilane SAM using an ink-free method. In this versatile method, both "positive" and "negative" type pattern transfers are possible. The chemically converted patterns are induced by localized electrical fields on the microcontacted areas, and the patterning resolution is insensitive to the diffusion of oxidizing agents because of the self-limiting oxidation kinetics, thereby enabling high-resolution, large-scale parallel patterning.

Introduction

Nanoparticles are fundamental building elements for a variety of applications in nanotechnology. Among available synthetic routes for nanoparticles, the colloidal chemistry methods are particularly suitable for nanoparticle device applications because of their control in sizes, shapes, compositions, and surface functionalities of synthesized nanoparticles.[1,2] Recently, there has been an increasing interest in organized self-assembly of two-dimensional (2D) colloid nanoparticle arrays because of the potentially important applications in addressable, combinatorial arrays for chemical and biological detection,[3−5] surface plasmonic devices,[6,7] and functional templates for assembly and growth of nanomaterials, nanocatalysts, and biologically active arrayed substrates.[1] It is well established that the stability of colloidal suspensions comes from the repulsive Coulomb interactions between the like-charged nanoparticles in sols. Thus, it is a natural strategy to utilize charge-patterned templates in the oppositely charged state for the organized assembly of colloidal nanoparticles onto solid supports from the liquid phase.[8] In the past few years, there have been several demonstrated approaches for electrostatic assembly of nanoparticles using microcontact printing (μCP) of charged self-assembled monolayers (SAMs)[9,10] and polyelectrolytes[11] as well as microcontact charging of electret thin films.[12] At present, μCP is one of the most promising approaches for controlled assembly because it can be applied for multiple-length-scale, parallel (fast) printing of a variety of functional inks, which can be used as linker agents for assembling nanoobjects.[13,14] However, the resolution of microcontact-based direct printing, including μCP and dip-pen nanolithography (DPN, a high-resolution, serial process, ref 15), is subject to lateral diffusion and is determined by the ink material, contact time, properties of the contact surfaces, and ambient conditions (temperature, humidity, etc.).[16,17]

Here, we present an alternative approach for controlled assembly of gold colloidal nanoparticles using electric-field-induced microcontact electrochemical conversion (MEC) of preassembled aminosilane monolayers. In this scheme, both the vertical and lateral electrochemical conversion rates (height/time, width/time) follow a self-limiting kinetics (the converted region forms a diffusion barrier for further conversion), such that these conversion rates drop exponentially with the contact time. As a result, the lateral resolution is insensitive to the molecular type and the contact time, enabling a high-resolution, high-reproducibility process. In addition, the electric-field-induced MEC method has the distinctive advantages of excellent controllability via the applied electric field and the possibility of large-scale and hierarchical parallel patterning.

In the past, several scanning-probe-induced local electrochemical conversion techniques via the liquid meniscus formed at the tip and sample junction have been demonstrated. For example, there have been reports of scanning-probe-induced local anodic oxidation of a variety of materials via tip−sample water meniscus formed under ambient conditions, such as Si to SiO_x,[18−20] TiN to TiO_x,[21] Si_3N_4 to SiO_x,[22] and local oxidation[23,24]

* Author to whom correspondence should be addressed. E-mail: gwo@phys.nthu.edu.tw.

(1) Shipway, A. N.; Katz, E.; Willner, I. *ChemPhysChem* **2000**, *1*, 18−52.
(2) *Colloids and Colloidal Assemblies*; Caruso, F., Ed.; Wiley-VCH: Weinheim, Germany, 2004.
(3) Freeman, R. G.; Grabar, K. C.; Allison, K. J.; Bright, R. M.; Davis, J. A.; Guthrie, A. P.; Hommer, M. B.; Jackson, M. A.; Smith, P. C.; Walter, D. G.; Natan, M. J. *Science* **1995**, *267*, 1629−1632.
(4) Okamoto, T.; Yamaguchi, I.; Kobayashi, T. *Opt. Lett.* **2000**, *25*, 372−374.
(5) He, L.; Musick, M. D.; Nicewarner, S. R.; Salinas, F. G.; Benkovic, S. J.; Natan, M. J.; Keating, C. D. *J. Am. Chem. Soc.* **2000**, *122*, 9071−9077.
(6) Barnes, W. L.; Dereux, A. Ebbesen, T. W. *Nature* **2003**, *424*, 824−830.
(7) Maier, S. A.; Atwater, H. A. *J. Appl. Phys.* **2005**, *98*, 011101.
(8) Tzeng, S.-D.; Lin, K.-J.; Hu, J.-C.; Chen, L.-J.; Gwo, S. *Adv. Mater* **2006**, *18*, 1147−1151.
(9) Tien, J.; Terfort, A.; Whitesides, G. M. *Langmuir* **1997**, *13*, 5349−5355.
(10) Aizenberg, J.; Braun, P. V.; Wiltzius, P. *Phys. Rev. Lett.* **2000**, *84*, 2997−3000.
(11) Chen, K. M.; Jiang, X.; Kimerling, L. C.; Hammond, P. T. *Langmuir* **2000**, *16*, 7825−7834.
(12) Jacobs, H. O.; Whitesides, G. M. *Science* **2001**, *291*, 1763−1766.
(13) Xia, Y.; Whitesides, G. M. *Angew. Chem., Int. Ed.* **1998**, *37*, 551−575.
(14) Gates, B. D.; Xu, Q.; Stewart, M.; Ryan, D.; Wilson, C. G.; Whitesides, G. M. *Chem. Rev.* **2005**, *105*, 1171−1196.
(15) Piner, R. D.; Zhu, J.; Xu, F.; Hong, S.; Mirkin, C. A. *Science* **1999**, *283*, 661−663.
(16) Sheehan, P. E.; Whitman, L. J. *Phys. Rev. Lett.* **2002**, *88*, 156104.
(17) Weeks, B. L.; Noy, A.; Miller, A. E.; De Yoreo, J. J. *Phys. Rev. Lett.* **2002**, *88*, 255505.
(18) Dagata, J. A.; Schneir, J.; Harary, H. H.; Evans, C. J.; Postek, M. T.; Bennet, J. *Appl. Phys. Lett.* **1990**, *56*, 2001−2003.
(19) Avouris, Ph.; Hertel, T.; Martel, R. *Appl. Phys. Lett.* **1997**, *71*, 285−287.
(20) Calleja, M.; García, R. *Appl. Phys. Lett.* **2000**, *76*, 3427−3429.
(21) Gwo, S.; Yeh, C.-L.; Chen, P.-F.; Chou, Y.-C.; Chen, T. T.; Chao, T.-S.; Hu, S.-F.; Huang, T.-Y. *Appl. Phys. Lett.* **1999**, *74*, 1090−1092.

10.1021/la060656r CCC: $33.50
Published on Web 08/05/2006

or conversion[25−27] of function groups of SAMs. Very recently, Garcia et al. have also demonstrated scanning-probe-induced local conversion via organic liquid menisci (e.g., Si to SiC_x using ethanol).[28] Using these scanning-probe-induced local conversion techniques, organized assemblies of various colloidal nanoparticles have been demonstrated onto scanning-probe-patterned SAMs.[29−34] In these scanning-probe techniques, the patterning process is realized by reactant (e.g., hydroxyl ions in the water meniscus) transport through the liquid meniscus at the tip and sample junction. Therefore, these are diffusion-limited processes. At present, high-resolution and high-packing-density local electrochemical conversion has been demonstrated for patterning oxide dot arrays (1.6 Tbit/in^2, 8-nm bits at a 20-nm pitch).[35] Furthermore, the self-limiting nature of conversion kinetics has been confirmed.[19,20,36−38] The remaining hurdles for local electrochemical conversion techniques are small patterning area and slow writing speed, which is limited by the reactant transport process. Therefore, the typical line writing speed is in the range of 0.1−10 μm/s and the dot writing time is in the range of a few ms to tens of s per dot (size-dependent) under ambient conditions. Recent breakthroughs of large-area electrochemical conversion using microcontact stamps[39−41] make it a viable approach to overcome the patterning-area and throughput limitations. In this paper, we exploit this approach for parallel electrostatic assembly of colloidal nanoparticles.

Experimental Methods

Stamp Fabrication. Both "positive" and "negative" type microcontact stamps were used in the experiments. Figure 1 shows schematically a process utilizing a negative-type microcontact stamp, while Figure 2a is a schematic representation of a process utilizing a positive-type microcontact stamp. For our experiment, stamps (~1 × 2 cm^2) were made from *p*-type Si(111) wafers (resistivity < 1 Ω·cm). The positive-type stamp was fabricated by photolithography. After resist development, the stamp was etched using a reactive ion-etching (RIE) instrument (Plasmalab 80 Plus, Oxford Instruments) with SF_6/O_2 plasma (flow rate: 30/6 sccm, 150 mTorr) at 225 W RF power for 30 s. The structure of the positive-type stamp was a square array of Si pillars with the following parameters (diameter and height are mean values over six pillars): 11.7 ± 0.3 μm diameter, 25 μm pitch, and 460 ± 30 nm depth (schematically shown in Figure 2a). For the negative-type stamps (for results shown in Figures 3 and 5), square arrays of ~45-nm-diameter, 530-nm-pitch holes were first patterned by electron beam lithography on the PMMA resists. Then, the negative-type stamps were fabricated by RIE with identical operating conditions as the positive-type stamp except that the etching time is 20 s. The stamp surfaces used for the MEC process were hydrophilic. The Si samples (~1 × 2 cm^2) which were imprinted on by the stamps were also cut from the same kind of Si wafers as the stamp materials.

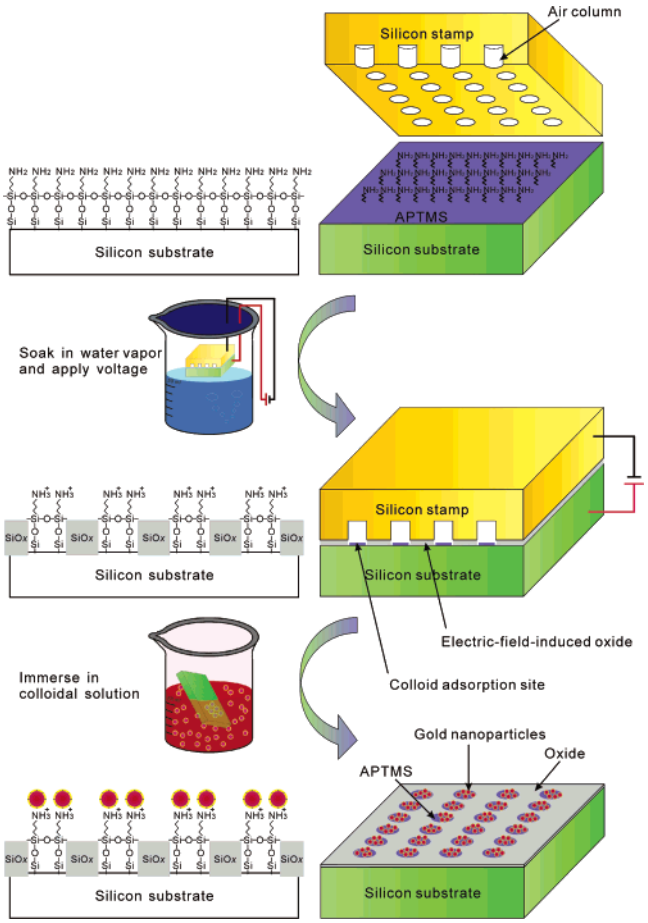

Figure 1. Parallel electrostatic assembly of 2D nanoparticle arrays via the MEC process. Schematic illustration of site-controlled adsorption of nanoparticle arrays onto a Si substrate preassembled with a (3-aminopropyl)trimethoxysilane (APTMS) monolayer and patterned using a negative-type Si microcontact electrochemical conversion (MEC) stamp. During the MEC process, conductive stamp and substrate are mechanically held together and are suspended in a sealed beaker filled with a supersaturated water vapor. The applied positive voltage on the substrate is a few V (relative to the stamp) and the contact time is a few min. After this electrochemical conversion step, an oxide pattern is created on the surface region contacted by the stamp. Finally, the patterned substrate is immersed in an aqueous solution of colloidal nanoparticles to form a 2D square lattice of nanoparticle arrays on APTMS-covered disks.

Aminosilane Monolayers and Colloids. Before the MEC patterning process, the nanoparticle adsorption templates were preassembled with a (3-aminopropyl)trimethoxysilane [APTMS, $H_2N(CH_2)_3Si(OCH_3)_3$, Aldrich, product no. 281778] monolayer. An aqueous solution of Au colloids was used for the selective adsorption experiments (10-nm mean diameter, ~0.01%, Sigma, product no. G1527). To deposit the APTMS monolayer, the Si substrate was first cleaned by deionized water and pure ethanol. Then, Si substrate was activated by air plasma (XEI Scientific) at 0.6 Torr and 10 W RF power for 10 min. After this process, the Si substrate surface was terminated by hydroxyl groups. Next, the substrate was immersed in a container filled with liquid-phase APTMS (97%) and was sealed

(22) Chien, F. S.-S.; Chang, J.-W.; Lin, S.-W.; Chou, Y.-C.; Chen, T. T.; Gwo, S.; Chao, T.-S.; Hsieh, W.-F. *Appl. Phys. Lett.* **2000**, *76*, 360−362.
(23) Sugimura, H.; Nakagiri, N. *Langmuir* **1995**, *11*, 3623−3625.
(24) Sugimura, H.; Hanji, T.; Hayashi, K.; Takai, O. *Adv. Mater.* **2002**, *14*, 524−526.
(25) Maoz, R.; Cohen, S. R.; Sagiv, J. *Adv. Mater.* **1999**, *11*, 55−61.
(26) Maoz, R.; Frydman, E.; Cohen, S. R.; Sagiv, J. *Adv. Mater.* **2000**, *12*, 725−731.
(27) Sugimura, H. *Jpn. J. Appl. Phys.* **2004**, *43*, 4477−4481.
(28) Tello, M.; García, R.; Martín-Gago, J. A.; Martínez, N. F.; Martín-González, M. S.; Aballe, L.; Baranov, A.; Gregoratti, L. *Adv. Mater.* **2005**, *17*, 1480−1483.
(29) Sugimura, H.; Nakagiri, N. *J. Am. Chem. Soc.* **1997**, *119*, 9226−9229.
(30) Hoeppener, S.; Maoz, R.; Cohen, S. R.; Chi, L.; Fuchs, H.; Sagiv, J. *Adv. Mater.* **2002**, *14*, 1036−1041.
(31) Masuda, Y.; Itoh, M.; Yonezawa, T.; Koumoto, K. *Langmuir* **2002**, *18*, 4155−4159.
(32) Li, Q.; Zheng, J.; Liu, Z. *Langmuir* **2003**, *19*, 166−171.
(33) Wouters, D.; Schubert, U. S. *Langmuir* **2003**, *19*, 9033−9038.
(34) Lin, X.; Zhu, X.; Zhang, J.; Zhu, T.; Liu, M.; Tong, L.; Liu, Z. *J. Phys. Chem. B* **2005**, *109*, 2657−2665.
(35) Cooper, E. B.; Manalis, S. R.; Fang, H.; Dai, H.; Matsumoto, K.; Minne, S. C.; Hunt, T.; Quate, C. F. *Appl. Phys. Lett.* **1999**, *75*, 3566−3568.
(36) Chien, F. S.-S.; Chou, Y. C.; Chen, T. T.; Hsieh, W.-F.; Chao, T.-S.; Gwo, S. *J. Appl. Phys.* **2001**, *89*, 2465−2472.
(37) Wouters, D.; Willems, R.; Hoeppener, S.; Flipse, C. F. J.; Schubert, U. S. *Adv. Funct. Mater.* **2005**, *15*, 938−944.
(38) Yang, M.; Zheng, Z.; Liu, Y.; Zhang, B. *J. Phys. Chem. B* **2006**, *110*, 10365−10373.
(39) Cavallini, M.; Mei, P.; Biscarini, F.; García, R. *Appl. Phys. Lett.* **2003**, *83*, 5286−5288.
(40) Yokoo, A. *J. Vac. Sci. Technol., B* **2003**, *21*, 2966−2969.
(41) Farkas, N.; Comer, J. R.; Zhang, G.; Evans, E. A.; Ramsier, R. D.; Wight, S.; Dagata, J. A. *Appl. Phys. Lett.* **2004**, *85*, 5691−5693.

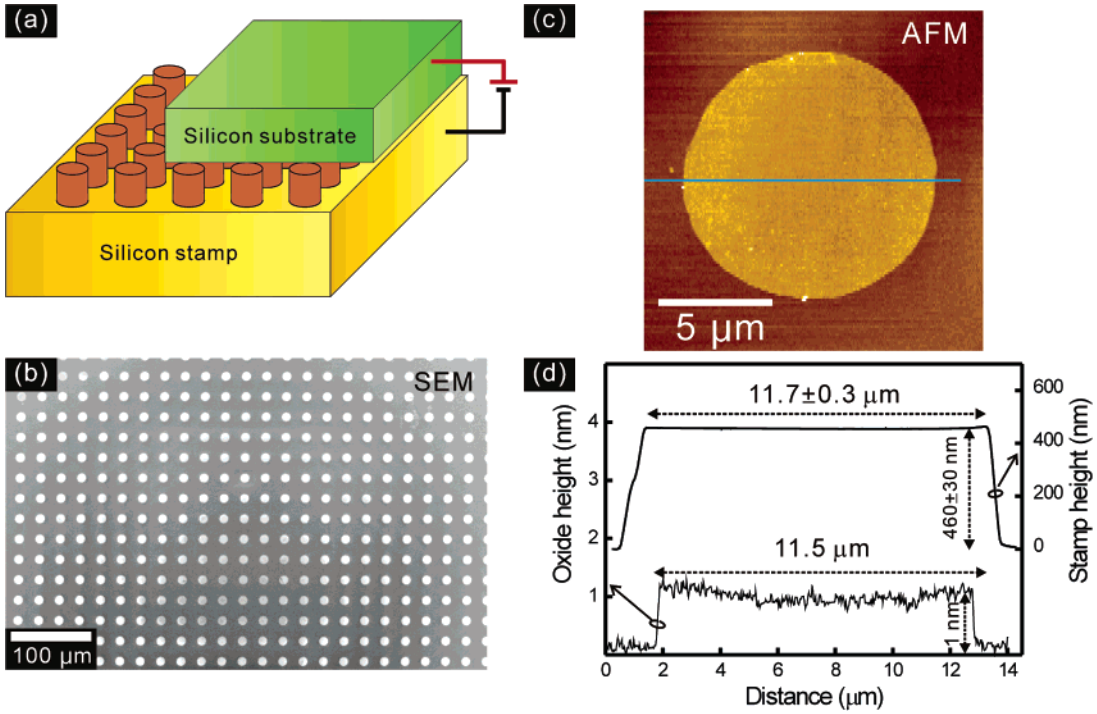

Figure 2. Positive-type MEC pattern transfer. (a) Schematic illustration of the MEC process on a native silicon substrate using a positive-type Si microcontact stamp. (b) Scanning electron microscopy (SEM) image of the oxide pattern created by the microcontact stamp shown above. (c) Atomic force microscopy (AFM) topographic image of a single oxide disk. (d) AFM line profiles of silicon microcontact stamp and resulting oxide pattern. The lateral dimension of the silicon cylinders on the stamp is given by the mean diameter measured from six Si cylinders.

with nitrogen for more than 24 h. Then, the Si substrate was cleaned by pure ethanol again to remove the residual APTMS molecules. For Au colloid adsorption, the Si substrate covered by a patterned APTMS monolayer was immersed into the aqueous Au colloidal solution for 30 min to form adsorption-site-controlled Au nanoparticle arrays.

Procedure for Microcontact Electrochemical Conversion (MEC). During the process of MEC, the substrate to be patterned was mechanically held together with the stamp (positive- or negative-type) using a clip. The stamp and substrate combination was suspended in a beaker containing some amount of hot water to maintain an oversaturated humidity. In addition, the beaker was sealed with a plastic film. After soaking in the water vapor, there were water menisci formed in the contact gaps between the substrate and the stamp. To create the anodic oxide patterns, we applied an electric bias using a constant-current power source (substrate positively biased relative to the stamp). The current was ~1.0−1.5 A at 6−10 V and the contact time was ~3−5 min. The resulting oxide pattern was insensitive to the contact time because of the self-limiting nature of conversion kinetics.

Scanning Electron Microscopy (SEM). SEM images of the oxide patterns and selectively adsorbed 2D colloidal structure were taken using a field-emission scanning electron microscope manufactured by Zeiss (model: Ultra 55). The presented images were obtained with an in-lens secondary-electron detector to achieve high-contrast surface imaging. We found that a clear SEM imaging contrast between converted and unconverted surface regions after the local anodic oxidation process was due to the differences in topographic height and charging.

Results and Discussions

Au nanoparticles formed by the reduction of $AuCl_4^-$ with trisodium citrate are negatively charged because of the adsorption of anion species in the aqueous colloidal suspension.[42−44] When the APTMS-monolayer-covered surface is immersed into the Au colloidal suspension, the terminal amino groups are protonated ($-NH_2 \rightarrow -NH_3^+$) in the suspension used here (the pH value ≈ 6.25).[42] Therefore, negatively charged Au nanoparticles can be assembled by electrostatic interaction onto the patterned APTMS monolayer with positively charged amino groups.

In practice, binary SAM systems with different terminal functional groups and colloid affinities are necessary to facilitate selective adsorption of charged colloids onto patterned SAM adsorption templates. In a recent μCP experiment[44] using a poly(dimethyl)siloxane (PDMS) stamp with protruding features (3-μm diameter circles), a $-CH_3$ terminated SAM was first printed on the substrate to create a nonadsorbing region for colloidal nanoparticles and an $-NH_2$ terminated SAM was subsequently coated on the unprinted surface region. Using the affinity difference of $-NH_2/-CH_3$, colloidal nanoparticles can be bound electrostatically with the $-NH_2$ terminated region.

However, the binary SAM systems require more process steps and can result in reduced process reliability. Furthermore, the problem of forming a mixed SAM ($-NH_2/-CH_3$) on the stamp-contacted region during the second $-NH_2$ terminated SAM coating step can significantly reduce the adsorption selectivity.[44] Therefore, a single $-NH_2$ terminated SAM is preferred for selective colloid adsorption if the processing technique allows. The MEC method reported here can allow for such a possibility because the electric-field-induced oxide region does not exhibit affinity for charged colloids and can function as the $-CH_3$ terminated region. In this work, we show that negative-type[45] pattern transfer is possible using the MEC technique. Thus, a

(42) Zhang, H.; He, H.-X.; Wang, J.; Mu, T.; Liu, Z.-F. *Appl. Phys. A* **1998**, *66*, S269−S271.

(43) Gole, A.; Sainkar, S. R.; Sastry, M. *Chem. Mater.* **2000**, *12*, 1234−1239.

(44) He, H. X.; Zhang, H.; Li, Q. G.; Zhu, T.; Li, S. F. Y.; Liu, Z.-F. *Langmuir* **2000**, *16*, 3946−3851.

(45) The definition of positive-type stamp is that the functional regions (e.g., selective etch masks, selective adsorption templates, etc.) of the stamp-patterned SAMs correspond to the *microcontacted* areas, while for the negative-type stamp the functional regions correspond to the *noncontacted* areas.

simple and robust process is possible to fabricate 2D colloid arrays on solid substrates.

Figure 1 shows the MEC scheme used by us for site-controlled adsorption of colloidal nanoparticles with a negative-type stamp. At first, the Si substrate was preassembled with an APTMS overlayer. Subsequently, by using the MEC process, the Si substrate was patterned with a negative-type stamp. In this process, the large applied electric field induced an electrochemical reaction which can result in the local damage of the contacted APTMS regions and the formation of an oxide pattern on the surface. According to a local electrochemical conversion (scanning probe oxidation) study performed by Sugimura et al.,[46] the SAM molecules (octadecyltrimethoxysilane) are first decomposed by intense electric field. Subsequently, under the intense electric field, the hydroxyl ions in the water meniscus diffuse through the remaining SAM molecules and the surface oxide layer. The second step can result in field-induced oxidation of the underlying silicon. Finally, the APTMS molecules on the oxide surface are completely decomposed and the anodic oxidation continuously progresses. Although recent investigations indicate that the scanning probe oxidation process on organic-monolayer-covered silicon is more complex than that on bare silicon substrates,[37,38] it has been confirmed that the final stage oxidation rate (after the organic molecules are completely degraded, as in our case) follows the exponential relationship previously reported for the scanning probe oxidation process of bare Si substrates.[38] In our experiment, under the positive biasing condition of APTMS-covered sample (during the microcontact process), the decomposed APTMS molecules with positively charged amino groups are repulsed away from the sample and are incorporated into the water meniscus. Although the decomposed APTMS molecules might be attracted to the stamp during the microcontact process, we do not expect the formation of strong chemical binding because of the lack of silane group on most of the decomposed APTMS molecules. Therefore, they could be removed readily after the electric field is turned off. Indeed, we have found that the hydrophilicity of the stamp was not changed after the microcontact process, implying that the stamp surface was not modified by the MEC process.

After this MEC process, the patterned substrate was immersed into the aqueous colloidal solution to form adsorption-site-controlled 2D nanoparticle arrays. Figure 2a shows schematically the MEC process using the positive-type stamp for patterning a square lattice of oxide disks on a native Si substrate surface (without the APTMS overlayer and any special surface treatment). Figure 2b is the SEM image of the resulting oxide pattern (after the MEC process) with a large imaging region of 0.5×0.4 mm^2. The brighter areas correspond to the patterned oxide regions. This SEM image demonstrates the excellent process uniformity over a large area ($\sim$mm^2 using the present setup, see Experimental Methods). After the MEC process, all of the patterned oxide disks have a nearly identical diameter of $\sim$11.5 μm. Figure 2c and d shows the atomic force microscopy (AFM) topographic image and line profile of a single oxide disk on the same oxide pattern. For comparison, the AFM line profile of a single Si pillar on the Si stamp is also shown (the width of the top plateau: 11.7 ± 0.3 μm; height of the pillar: 460 ± 30 nm; the given values are mean values over six pillars). The widths of the oxide disk and the Si pillar plateau are in excellent agreement, indicating a high-fidelity pattern transfer. In addition, the structure of oxide topography appears to be quite uniform over the whole oxide disk and the oxide disk wall is very abrupt, showing no significant lateral diffusion (wall width $<$ 100 nm, comparable with the reported local electrochemical conversion results). These results demonstrate that the patterning resolution is insensitive to the diffusion of oxidizing agents because of the self-limiting kinetic. Determined from this AFM topographic image, the oxide height is only about 1 nm, indicating that the surface contrast obtained by SEM (Figure 2b) is quite sensitive.

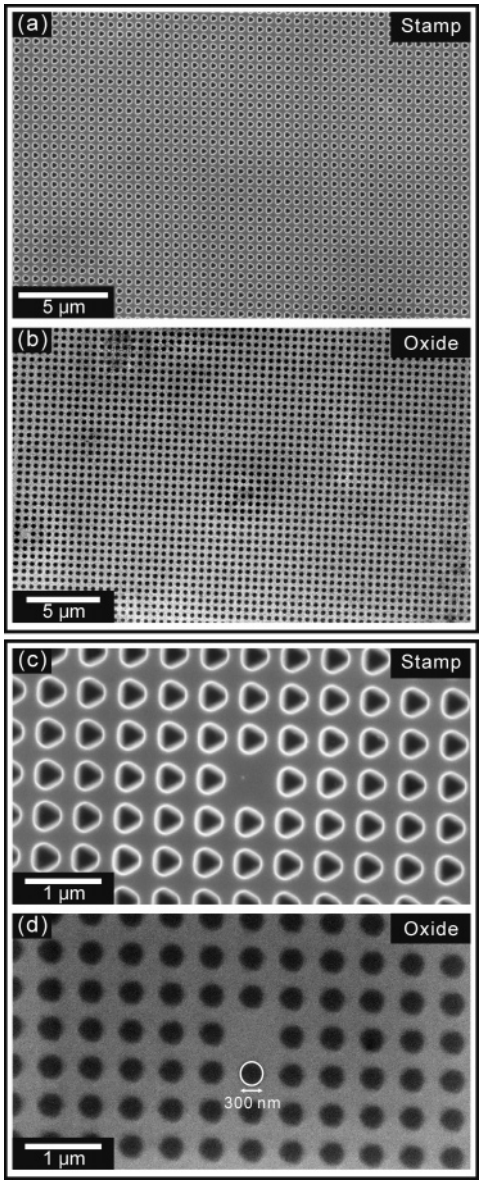

Figure 3. Negative-type MEC pattern transfer. (a) Large-area SEM image of a negative-type Si MEC stamp. It consists of a square lattice of inverted pyramids on a Si(111) substrate created by reactive ion etching (RIE). (b) Large-area SEM image of an oxide pattern created by the MEC process on a native Si substrate. The oxide pattern (bright area in SEM image) is formed by using the negative-type Si MEC stamp shown in a. (c) High-magnification SEM image of the stamp. The inverted triangular pyramid shape of the RIE-etched hole can be clearly seen. Note that there is a point defect at the center of the image. (d) High-magnification SEM image of the corresponding oxide pattern after the MEC process. The defect on the stamp is faithfully transferred to the oxide pattern.

Figure 3a shows an SEM image (25×17 μm^2) of one of the negative-type stamps used for the MEC experiments. Figure 3b displays a large scanning area (30×20 μm^2) SEM image of the resulting oxide pattern after the MEC process on a native Si substrate surface (without the APTMS overlayer and special surface treatment). This image demonstrates that excellent

(46) Sugimura, H.; Hanji, T.; Hayashi, K.; Takai, O. *Ultramicroscopy* **2002**, *91*, 221−226.

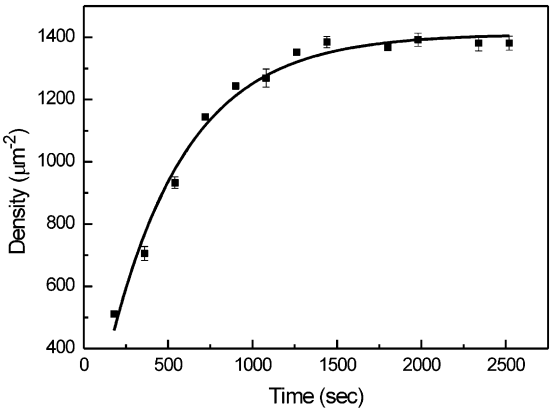

Figure 4. SEM images are used to quantify the extent of colloidal nanoparticle adsorption onto unpatterned, pristine APTMS SAMs. The number of Au nanoparticles per square micrometer (average ± standard deviation) is obtained by counting nanoparticles in five different areas (1.5 × 1.5 square micrometer). From a series of related experiments, we find that the nanoparticle adsorption rate drops exponentially with the immersion time and eventually reaches zero at a saturation nanoparticle density (as indicated by the fitting curve).

uniformity of the oxide pattern over a large area can also be obtained with the negative-type stamp. Figure 3c shows the SEM image on part of the stamp with a missing hole (defect). This defect was precisely transferred to the oxide pattern (Figure 3d). Because the reactive ion etching (RIE) process used for fabricating the negative-type stamp is anisotropic in nature, triangular-shaped etching structures were observed on the stamp surface. These triangles correspond to the boundary intercepted with the (111) surface plane by the inverted triangular pyramid formed by three {111} facets. The depth of the inverted triangular pyramid estimated from the geometric relation is ∼240 nm. Although the etched geometry is an inverted triangular pyramid, the boundary of the oxide pattern shown in Figure 3d still exhibits a nearly perfect circle shape (∼300 nm in diameter). A hypothesis for this phenomenon is that the surface tension of the water meniscus at the contact interface might cause the final circular oxide aperture.

Following the negative-type MEC processes described in Figure 1, Au nanoparticle arrays selectively adsorbed on the APTMS-covered areas can be prepared (see detailed procedure in Experimental Methods). To understand better the adsorption kinetics, Figure 4 shows the number of adsorbed Au nanoparticles on unpatterned, pristine APTMS monolayers as a function of the adsorption time. From a series of related experimental results, we concluded that the nanoparticle adsorption rate drops exponentially with the immersion time and eventually reaches zero at a saturation nanoparticle density (as indicated by the fitting curve).[47] It has also been found that the areal density of adsorbed Au nanoparticles depends on the pH value, particle size, particle concentration, and ionic strength of the colloidal suspension.[42−44] According to this control experiment, we concluded that an adsorption time of 30 min is sufficient to reach the saturation nanoparticle coverage for the specific Au sol used here. Besides, we have found that the saturation density of absorbed Au nanoparticles was 1410 ± 20 nanoparticles per μm^2 area using an unpatterned, pristine APTMS monolayer.

Using the parameters found in the control experiment, we have performed site-controlled adsorption of Au nanoparticles on an MEC-patterned APTMS monolayer. Figure 5a and b displays the low- and medium-magnification SEM images of

(47) Tzeng, S.-D.; Lin, M.-H.; Gwo, S., unpublished data.

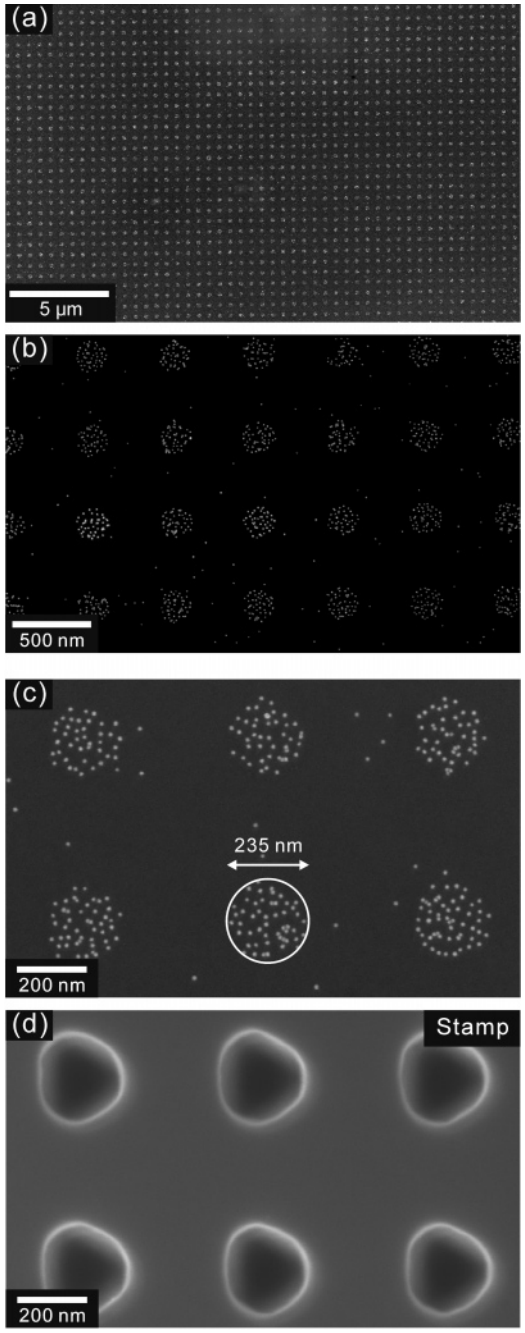

Figure 5. (a−c) SEM images of site-controlled adsorption of Au nanoparticle arrays. The Si substrate is preassembled with an APTMS monolayer before the MEC process. The average density of nanoparticles on the selectively adsorbed areas is 1080 ± 90 nanoparticles per μm^2 area. Also, ∼99% of Au nanoparticles are selectively adsorbed on the MEC-defined adsorption sites. (d) SEM image of the Si MEC stamp used for creating the nanoparticle adsorption template.

selectively adsorbed Au nanoparticle arrays. Figure 5c shows the high-magnification SEM image of 2 × 3 Au nanoparticle arrays. For comparison, Figure 5d shows the corresponding negative-type MEC Si stamp used for this patterning process (note that this stamp is different from the one shown in Figure 3a). This result demonstrates that on the noncontacted areas APTMS would not be decomposed at all and implies that MEC is a very proper technique to selectively modify SAMs. In Figure 5, the adsorbed Au nanoparticles are sparsely distributed and do not form a closely packed structure because of the repulsive interactions of charged gold nanoparticles on the APTMS

surface.[3−5] On the nanoparticle-adsorbed areas shown in Figure 5c, there are an average of 47 ± 4 Au nanoparticles on a 235-nm-diameter circle area. Thus, the average density of nanoparticles on the selectively adsorbed areas is 1080 ± 90 nanoparticles per μm^2 area, smaller than the nanoparticle surface coverage of ∼1400 nanoparticles per μm^2 area observed on the unpatterned, pristine APTMS-covered surface. We believe that the inconsistency in areal density of selectively adsorbed Au nanoparticles results from the boundary effect of ultrasmall APTMS regions. This is partly due to the difficulty in positioning the precise boundary. Also, the APTMS molecules on the boundary might be damaged during the microcontact process. That would cause the lower nanoparticle density on the circle area than that on the pristine APTMS surface. To demonstrate this boundary effect, we select 150-nm-diameter inner circle areas for additional density analysis of selectively adsorbed Au nanoparticles. We find that an average of 24 ± 2 Au nanoparticles adsorb on a 150-nm-diameter circle over 20 inner areas shown in Figure 5b. Thus, the average density of nanoparticles adsorbed on the inner circle areas is 1360 ± 120 nanoparticles per μm^2 area, in good agreement with the nanoparticle surface coverage of ∼1400 nanoparticles per μm^2 area observed on the unpatterned, pristine APTMS-covered surface. There are also some "strayed" nanoparticles attached on the oxide region (as shown in Figure 5c). This is probably due to the existence of either residual APTMS molecules on the contacted region or some unidentified impurity- or defect-induced binding sites on the surface. The reason for the existence of residual APTMS might be that some decomposed APTMS molecules in the MEC process retain their silane groups and attach back to the stamp-oxidized region. Nevertheless, the coverage of the Au nanoparticles on the oxide-covered region is only about 16 nanoparticles per μm^2 area. Therefore, this process exhibits a high-adsorption selectivity of ∼99% for Au colloidal nanoparticles.

Conclusions

We have found that the parallel process of microcontact electrochemical conversion is a reliable patterning method for large-area, high-resolution organized assembly of colloidal nanoparticle arrays onto charged SAMs. Compared to the conventional parallel processes using microcontact printing of ink materials, this patterning method adopts a preassembled functional molecular monolayer and the electrochemical conversion kinetics exhibits a characteristic self-limiting behavior (insensitive to the contact time and molecular type). Thus, it is insensitive to the common problem of ink lateral diffusion and the resulting resolution degradation. Furthermore, we have demonstrated that negative-type pattern transfer can be performed with this method, resulting in reduced process steps and enhanced process reliability for site-controlled adsorption of nanoparticles using one conversion step and a single SAM. The dimensions of the adsorption site can be further reduced with finer nanofabricated stamps and, in principle, can be about a few nm. Besides the present application for assembly of nanoparticles, the reported methodology could become a general approach for the fabrication of site-controlled adsorption templates of functional molecules and biomacromolecules, using various combinations of microcontact liquid menisci and functional SAMs.

Acknowledgment. This work was supported in part by the National Nanoscience and Nanotechnology Project in Taiwan under contract no. NSC 95-2120-M-007-014.

LA060656R